Tokamak residual zonal flow level in near-separatrix region*

Shi Bing-Ren(石秉仁)†

Southwestern Institute of Physics, Chengdu 610041, *China*

(Received 10 November 2008; revised manuscript received 23 February 2010)

Residual zonal flow level is calculated for tokamak plasmas in the near-separatrix region of a diverted tokamak. A recently developed method is used to construct an analytic divertor tokamak configuration. It is shown that the residual zonal flow level becomes smaller but still keeps finite near the separatrix because the neoclassical polarisation mostly due to the trapped particles goes larger in this region.

Keywords: residual zonal flow, divertor configuration
PACC: 5225M, 5230, 5255G

1. Introduction

The $\boldsymbol{E}\times\boldsymbol{B}$ zonal flows are generally recognized to be significant for the reduction of turbulent transport either in tokamaks or in other toroidal plasma confinement systems.[1−9] This is an issue closely relevant to the confinement mode transition from low mode (L-mode) to high mode (H-mode), and the standard transition usually appears in the near-edge region. For most tokamak devices, such a transition happens in an equilibrium with divertor configuration.[10] Previously, Rosenbluth and Hinton provided an analytic study of the ion-temperature gradient (ITG) turbulence for tokamak plasmas and obtained an analytic formula for the residual zonal flow that is suitable for large aspect ratio circular tokamak plasma.[1] Later, non-circular shaping and arbitrary aspect ratio effects were considered[11,12] by using a simple analytic equilibrium model, the so-called Solov'ev configuration. However, for more relevant experimental cases, the residual zonal flow level in the divertor configuration is still not considered. Very recently, we suggested to use a semi-analytic simple model to describe the tokamak configuration with divertor separatrix[13] that lends us to conveniently calculate this residual zonal flow level in the near-separatrix region. We discuss such an equilibrium in Section 2 and calculate the residual zonal flow level in Section 3. The basic result obtained seems to indicate that the residual zonal flow is reduced much but still keeps finite in the near-separatrix region.

2. Model divertor configuration[13]

Tokamak equilibrium of up-down symmetry with D-shape divertor separatrix can be described by a semi-analytic model. In this model, the poloidal flux $\psi(R,Z)$ can be simply described by only two terms of separable solutions of the original Grad–Shafranov equation as follows:

$$\psi(R,Z)=\psi_{\rm a}[g_k(x)\cos(ky)+c_0g_0(x)]. \tag{1}$$

The poloidal magnetic field is determined by

$$\boldsymbol{B}_{\rm p}=\nabla\psi\times\nabla\zeta. \tag{2}$$

And (R, ζ, Z) is the cylindrical coordinates while $x=R/R_0$ and $y=Z/R_0$, with R_0 being the major radius of the equilibrium configuration. Function $g_k(x)$ is the solution of the following homogenous ordinary differential equation:

$$\frac{{\rm d}^2g_k}{{\rm d}x^2}-\frac{1}{x}\frac{{\rm d}g_k}{{\rm d}x}+(\eta\alpha+\eta\beta x^2-k^2)g_k=0, \tag{3}$$

while $g_0(x)$ is the solution of the following equation

$$\frac{{\rm d}^2g_0}{{\rm d}x^2}-\frac{1}{x}\frac{{\rm d}g_0}{{\rm d}x}+(\eta\alpha+\eta\beta x^2)g_0=0. \tag{4}$$

Equations (3) and (4) will be solved numerically in range $0<x_1\le x\le x_2$. Within this range, these ordinary differential equations are regular. We usually set $g_k(x_{10})=0$ and $g_k'(x_{10})=s_k$. The value of s_k is determined by such a condition as $\max\{g_k(x)\}=1$. Similarly, Eq. (4) is solved by setting $g_0(x_{11})=0$ with

*Project supported by the National Natural Science Foundation of China (Grant No. 10575037).
†Corresponding author. E-mail: shibr@swip.ac.cn
© 2010 Chinese Physical Society and IOP Publishing Ltd

$x_{11} \geq x_{10}$ and $g_0'(x_{11}) = s_0$. The s_0 value is also determined by $\max(g_0) = 1$. Parameter η is related to the central safety factor q_0 by $\eta = q_0^2/f_{\rm q}^2$ where $f_{\rm q} = 1/(x_{\rm m}\sqrt{g_{\rm m}''(x_{\rm m}) + c_0 g_0''(x_{\rm m})})$, with $x_{\rm m}$ being the position of the magnetic axis(prime denotes derivative with respect to x). Parameter α is the measure of the plasma paramagnetism ($\alpha > 0$) or diamagnetism ($\alpha < 0$) while $\beta = 2\mu_0 P_0/B_0^2$ is the central beta value of the plasma and the pressure is assumed to be a parabolic profile about the normalised poloidal flux: $P = P_0(\psi/\psi_{\rm a})^2$. Parameters k and c_0 are related to the elongation of the plasma cross-section. In this paper, for simplicity we select $x_{10} = x_{11} = x_1$ so that the vertical line $x = x_1$ will be automatically a sector of the boundary magnetic surface $\psi = 0$ which exhibits a D-shape structure. There is a null point at this boundary magnetic surface for the poloidal magnetic field where

$$\partial\psi/\partial x = g_k'(x_1)\cos(ky) + c_0 g_0'(x_1) = 0. \tag{5}$$

This condition means

$$y_{\rm X} = \frac{1}{k}\cos^{-1}\left[-\frac{c_0 g_0'(x_1)}{g_k'(x_1)}\right]. \tag{6}$$

With coefficient c_0 increasing from $c_0 = 0$ to a critical value $c_{0\rm c} = g_k'(x_1)/g_0'(x_1)$, the X-point moves away from $y_{\rm X} = \pi/2k$ to $y_{\rm X} = \pi/k$ and the elongation of the last closed magnetic surface, which is defined as the ratio of the area enclosed by this surface to the area of a circle that has a radius $(x_2 - x_1)/2$ where x_2 is the outmost major radius of the boundary surface, also increases gradually. For given $\eta\alpha, \eta\beta$ and k, the aspect ratio of the plasma cross-section, $A = (x_1 + x_2)/(x_2 - x_1)$ is determined by x_1 as shown in Fig. 1.

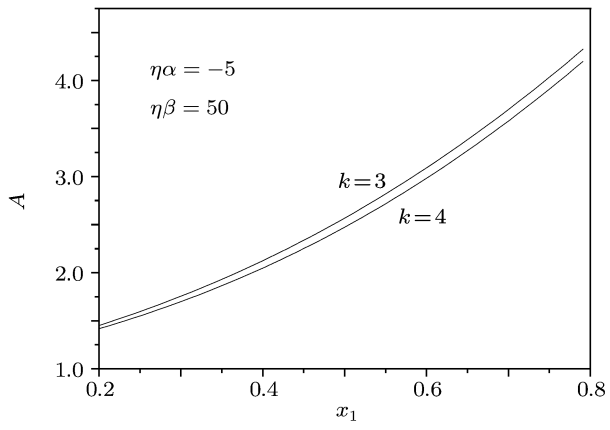


Fig. 1. Dependences of the aspect ratio $A = (x_1 + x_2)/(x_2 - x_1)$ on x_1 for $k = 3$, 4.

If we choose $c_0 = 0.99c_{0\rm c}$, the elongation of the boundary magnetic surface is plotted against x_1 in Fig. 2. In the near-magnetic axis region, the magnetic surface exhibits elliptic shape and its elongation is about $\kappa = \sqrt{-(g_{k\rm m}'' + c_0 g_{0\rm m}'')/k^2 g_{k\rm m}}$ that is larger than the elongation of the near boundary magnetic surface.

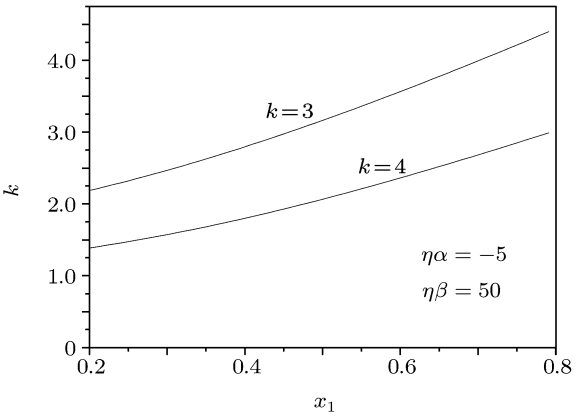


Fig. 2. Elongations of the last closed magnetic surface against x_1 for $k = 3$, 4.

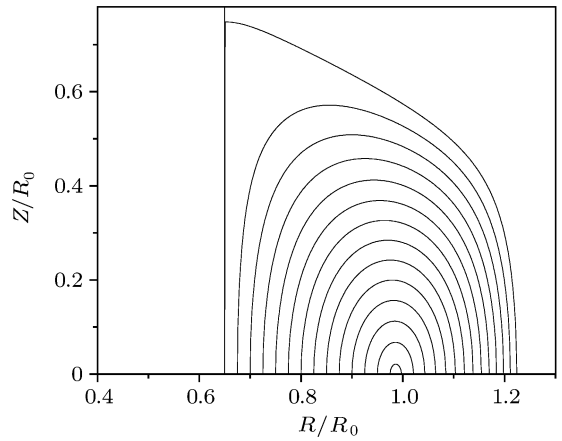


Fig. 3. Magnetic surface for equilibrium with parameters indicated in the text.

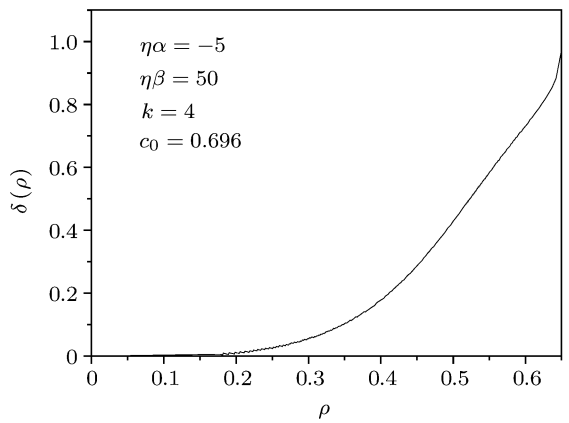


Fig. 4. Triangularity factor $\delta(\rho)$ against the average radius ρ for the equilibrium case shown in Fig.3.

From Fig. 2, we can set $x_1 = 0.65$ to obtain tokamak equilibrium with $A = 3.2$ and the allowable largest elongation $\kappa = 2.5$ for $k = 4$ and $c_0 = 0.696$. The configuration obtained in this way is shown in Fig. 3 and the corresponding variations of the triangularity and the elongation of magnetic surface against the average minor radius of that surface are shown in Figs. 4 and 5, respectively.

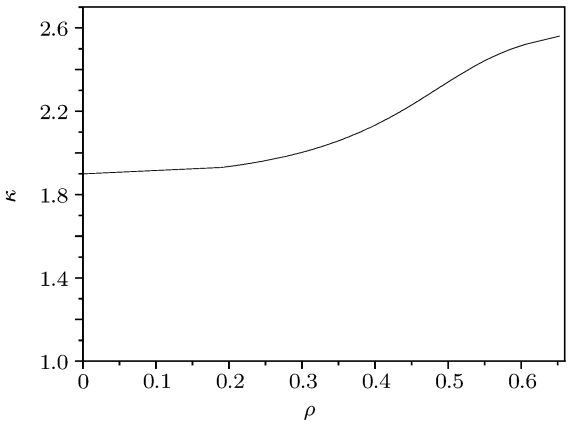


Fig. 5. Elongation against average minor radius for the configuration shown in Fig. 3.

3. Residual zonal flow level in near-separatrix region

As indicated by experiments and simulations, the residual zonal flows mainly appear in the edge region of tokamak plasmas. However, the previous analyses usually used the large aspect ratio approximation to obtain analytic results. Recently, for equilibrium of arbitrary aspect ratio and large elongation, we found that the residual zonal flow level can be expressed by a formula quite similar to that of the original Rosenbluth–Hinton if we define the safety factor q as the one for the circular cross-section case but with arbitrary aspect ratio.[12] In the present paper, we carry out a similar calculation for the equilibrium with double divertor structure described by semi-analytic solution.[13] The starting equation is the same as that in Refs. [11] and [12], i.e.,

$$\phi_{k,\mathrm{f}} = \phi_{k,0}/\Theta, \tag{7}$$

where ϕ_k is the Fourier component of the electric potential of the zonal flow, subscript 'f' and '0' represent the final state and the original state, respectively, Θ is the shield factor due to the neoclassical polarisation of ions[12] and expressed as

$$\Theta = 1 + \frac{(FS')^2}{\langle k_\perp^2 h^2\rangle}\left[\langle h^2\rangle - \frac{3}{2}A\int_0^{\lambda_1} g(\lambda)\mathrm{d}\lambda\right]. \tag{8}$$

Here, $h = B_0/B \approx x$, for the configuration of interest in this paper, i.e., the one that is described in the previous section, we have

$$\langle h^2\rangle = \oint \frac{x^3\sqrt{r^2+r_\theta^2}\mathrm{d}\theta}{\sqrt{(g_k'\cos(ky)+c_0g_0')^2+k^2\sin^2(ky)g_k^2}}/A, \tag{9}$$

$$A = \oint \frac{x\sqrt{r^2+r_\theta^2}\mathrm{d}\theta}{\sqrt{(g_k'\cos(ky)+c_0g_0')^2+k^2\sin^2(ky)g_k^2}}, \tag{10}$$

$$\begin{aligned}\langle k_\perp^2 h^2\rangle &= S'^2\langle h^2(\nabla\psi)^2\rangle = S'^2\left(\frac{\psi_\mathrm{a}}{R_0}\right)^2\langle h^2(\bar\nabla\bar\psi)^2\rangle \\ &= \frac{S'^2F^2}{\eta}\langle x^2[(g_k'\cos(ky)+c_0g_0')^2+k^2\sin^2(ky)g_k^2]\rangle \\ &= \frac{S'^2F^2}{\eta}\oint x^3\sqrt{(r^2+r_\theta^2)[(g_k'\cos(ky)+c_0g_0')^2+k^2\sin^2(ky)g_k^2}\mathrm{d}\theta/A,\end{aligned} \tag{11}$$

and the function

$$g(\lambda) = 1/\oint \frac{J\mathrm{d}\theta}{\sqrt{h(h-\lambda)}}, \quad 0 \le \lambda < \lambda_1 = x_1 \tag{12}$$

is related to the contribution of the trapped particles. Figure 6 shows the variations of function $g(\lambda)$ with λ for different selected values of ε.

Near the magnetic axis, we use the approximate analytic magnetic surface that exhibits elliptic cross-section and satisfies the following equation:

$$\frac{(x-x_\mathrm{m})^2}{a^2} + \frac{y^2}{b^2} = 1,$$

or

$$x = x_\mathrm{m} + a\cos t, \quad y = b\sin t \tag{13}$$

with

$$a = \sqrt{-\frac{2(\bar\psi_\mathrm{m}-\boldsymbol{\psi})}{(g_k''+c_0g_0'')}}, \quad b = \sqrt{\frac{2(\bar\psi_\mathrm{m}-\bar\psi)}{k^2g_k}}, \tag{14}$$

and along the poloidal projection of the magnetic field line we have

$$\mathrm{d}l/B_{\mathrm{p}} = x\mathrm{d}x/(-\partial\bar{\psi}/\partial y) = (xa\sin t/k^2 g_k(x) b\sin t)\mathrm{d}t = (xa/k^2 g_k b)\mathrm{d}t, \tag{15}$$

so that

$$\oint AJ\mathrm{d}\theta = \left(\frac{2a}{k^2 g_k(x_{\mathrm{m}})b}\right)\int_0^{\pi} Ax\mathrm{d}t = \frac{2x_{\mathrm{m}}}{k\sqrt{-g_k(g_k''+c_0 g_0'')}}\int_0^{\pi} A(1+\varepsilon\cos t)\mathrm{d}t = 2f_q x_{\mathrm{m}}^2\int_0^{\pi} A(1+\varepsilon\cos t)\mathrm{d}t, \tag{16}$$

$$\oint J\mathrm{d}\theta = 2f_q x_{\mathrm{m}}^2\pi, \tag{17}$$

$$\langle h^2\rangle = \frac{1}{\pi}\int_0^{\pi}(1+\varepsilon\cos t)^3\mathrm{d}t, \tag{18}$$

$$\begin{aligned}\langle h^2(\bar{\nabla}\bar{\psi})^2\rangle &= \frac{2(\bar{\psi}_{\mathrm{m}}-\bar{\psi})}{\pi}\left[(g_k''+c_0 g_0'')\int_0^{\pi}(1+\varepsilon\cos t)^3\cos^2 t\,\mathrm{d}t + k^2 g_k\int_0^{\pi}(1+\varepsilon\cos t)^2\sin^2 t\,\mathrm{d}t\right]\\ &= 4(\bar{\psi}_{\mathrm{m}}-\bar{\psi})^2[I_1/a^2 + I_2/b^2],\end{aligned} \tag{19}$$

$$I_1 = \frac{1}{\pi}\int_0^{\pi}(1+\varepsilon\cos t)^3\cos^2 t\,\mathrm{d}t, \tag{20}$$

$$I_2 = \frac{1}{\pi}\int_0^{\pi}(1+\varepsilon\cos t)^3\sin^2 t\,\mathrm{d}t, \tag{21}$$

$$\begin{aligned}\frac{1}{g(\lambda)} &= \oint\frac{J\mathrm{d}\theta}{\sqrt{h(h-\lambda)}}\\ &= 2f_q x_{\mathrm{m}}^2\int_0^{\pi}\mathrm{d}t\sqrt{\frac{1+\varepsilon\cos t}{1+\varepsilon\cos t-\lambda}},\\ &\quad 0\le\lambda<1-\varepsilon,\end{aligned} \tag{22}$$

$$A\int_0^{\lambda_1} g(\lambda)\mathrm{d}\lambda = \int_0^{1-\varepsilon}\frac{\mathrm{d}\lambda}{\frac{1}{\pi}\int_0^{\pi}\mathrm{d}t\sqrt{\frac{1+\varepsilon\cos t}{1+\varepsilon\cos t-\lambda}}}. \tag{23}$$

In these equations, $\varepsilon = a/x_{\mathrm{m}}$. Finally we obtain

$$\begin{aligned}\Theta &= 1+\frac{q_0^2}{f_q^2\langle h^2(\bar{\nabla}\bar{\psi})^2\rangle}\left[\langle h^2\rangle - \frac{3}{2}A\int_0^{\lambda_1} g(\lambda)\mathrm{d}\lambda\right]\\ &= 1+\frac{q_0^2}{\varepsilon^2(\kappa^2 I_1 + I_2)}\left[\langle h^2\rangle - \frac{3}{2}A\int_0^{\lambda_1} g(\lambda)\mathrm{d}\lambda\right].\end{aligned} \tag{24}$$

The elongation has been defined already in Section 2. Inverse aspect ratio relevant functions $I_1(\varepsilon)$ and $I_2(\varepsilon)$ are shown in Fig. 7.

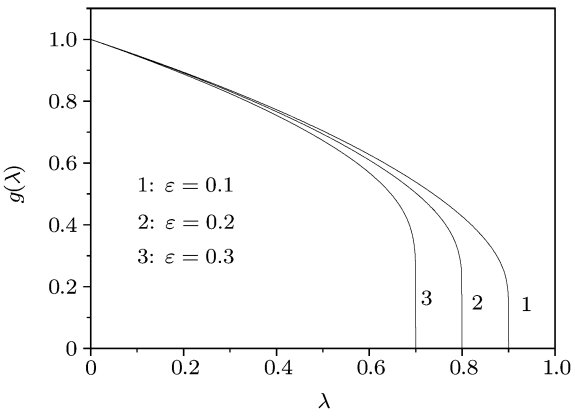


Fig. 6. Variations of $g(\lambda)$ with λ for three different values of ε.

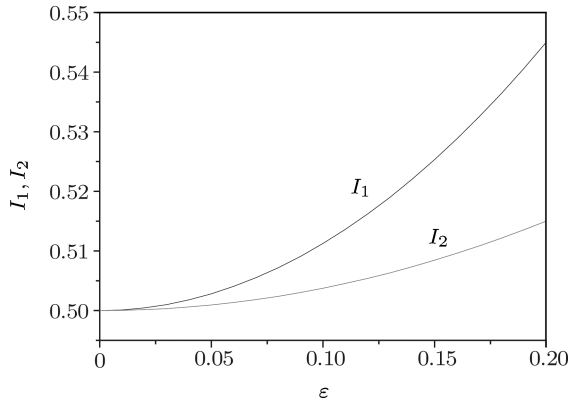


Fig. 7. Curves for $I_1-\varepsilon$ and $I_2-\varepsilon$.

In calculation, we use Eqs. (8)–(12) for $\varepsilon > 0.1$ and use Eqs. (15)–(24) for $\varepsilon < 0.1$. Using the above formulae, we can calculate the final result about the

shielding factor, and an example is shown in Fig. 8.

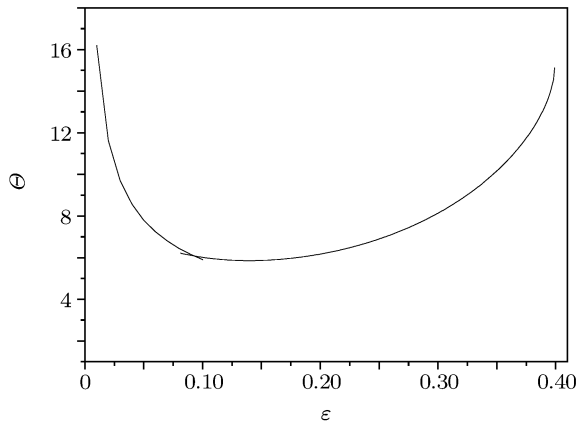


Fig. 8. Shielding factor Θ against ε for configuration parameters: $A = 2.502$, $\eta\alpha = -5$, $\eta\beta = 50$, $k = 5$, $c_0 = 0.4$.

The increase in shielding factor Θ (thus the decrease in residual zonal flow level), when ε decreases from about a value $\varepsilon = 0.1$, is generally observed in other similar analyses[11,14] and is the general result of neoclassical polarisation.[1] However, physically, this result is unreasonable because the limit $\varepsilon \to 0$ corresponds to a straight cylinder, however, the classical cylindrical physics has not been recovered (in cylindrical geometry, there appears no neoclassical polarisation), for which the reason may be considered from several aspects. One is that the long wave approximation that yields the basic Eq. (1) is invalid for $\varepsilon \to 0$ because the poloidal Larmor radius $\rho_{\rm p} = \rho_{\rm i} q/\varepsilon \to \infty$ so that the condition $Q = FS'v_{\parallel}/\Omega = k_{\perp}\rho_{\rm p} << 1$ in Refs. [1] and [11] is violated. The other reason is that the eikonal expression $f_k \propto \exp(\mathrm{i}\, kr)$ is an inappropriate choice for $\varepsilon \to 0$(the Laplacian ∇^2 can not be replaced by $-k_{\perp}^2$). Fortunately, we are interested in the region near the edge and the results for small values of ε are considered only as reference ones. In this paper, we do not discuss this issue in more detail.

Unlike the analytic configuration such as the Solov'ev solution[11,12] that permits a separation of the elongation from other parameters, now we can hardly do so. For equilibrium cited above, the change of elongation can result in change of other parameters like the triangularity. A clear trend is seen, however, that near a separatrix, the neoclassical shielding effect goes strong and the residual zonal flow level turns weak. This conclusion is somewhat discrepant to the general observation that zonal flows stabilize turbulence and make transition from the L-mode to the H-mode and a concomitant large decrease in edge electric field to a relatively large negative one.[10] Then more physics, we think, should be sought besides what has been discussed in recent studies regarding the zonal flows excited by ITG turbulence.

4. Discussion

We calculate the residual zonal flow level that originates from ITG turbulence and show that in the near-separatrix region of a diverted tokamak, it becomes rather weak. This calculation makes it possible to compare the zonal flow level with an experimentally relevant configuration and pose some questions on both the mechanism of the ITG zonal flow stabilisation and its role in the L–H transition because it is largely weakened by neoclassical polarisation of the trapped particle in this region.

References

[1] Rosenbluth M N and Hinton H 1998 *Phys. Rev. Lett.* **80** 728

[2] Hinton H and Rosenbluth M N 1999 *Plasma Phys. Contr. Fusion* **41** A653

[3] Jenko M A and Dorland 2002 *Phys. Rev. Lett.* **89** 225001

[4] Kim E, Holland C and Diamond P H 2003 *Phys. Rev. Lett.* **91** 075003

[5] Sugama H and Watanabe T H 2005 *Phys. Rev. Lett.* **94** 115001

[6] Sugama H and Watanabe T H 2006 *Phys. Plasmas* **13** 012501

[7] Watanabe T H and Sugama H 2006 *Nucl. Fusion* **46** 24

[8] Itoh K, Itoh S I, Diamond P H, Hahm T S, Tynan G R, Yagi M and Nagashima Y 2006 *Phys. Plasmas* **13** 055502

[9] Sugama H, Watanabe T H and Horton W 2007 *Phys. Plasmas* **14** 022502

[10] Wagner F 2007 *Plasma Phys. Contr. Fusion* **49** B1

[11] Xiao Y and Catto J P 2006 *Phys. Plasmas* **13** 082307

[12] Shi B R 2007 *Plasma Phys. Contr. Fusion* **49** 2019

[13] Shi B R 2008 *Plasma Phys. Contr. Fusion* **50** 085006

[14] Angelino P, Garbet X, Villard L, Bottino A, Jolliet S, Ghenfrih Ph, Grandgirad V, McMillan B F, Sarazin Y, Dif-Pradalier G and Tran T M 2008 *Phys. Plasmas* **15** 062306